S1. Supplementary Information

Robust substrate anchorages of silk lines with extensible nano-fibres

Jonas O. Wolff[1*,a], Daniele Liprandi[2,a], Federico Bosia[3], Anna-Christin Joel[4], and Nicola M. Pugno[2,5,]**

[1] Department of Biological Sciences, Macquarie University, Sydney, NSW 2109, Australia

[2] Laboratory of Bio-inspired, Bionic, Nano, Meta Materials & Mechanics, Department of Civil, Environmental and Mechanical Engineering, University of Trento, Via Mesiano 77, I-38123 Trento, Italy

[3] Department of Applied Science and Technology, Politecnico di Torino, Corso Duca degli Abruzzi 24, 10129, Torino, Italy

[4] Institute of Biology II, RWTH Aachen University, Worringerweg 3, 52074 Aachen

[5] School of Engineering and Materials Science, Queen Mary University, Mile End Rd, London E1 4NS, UK

* corresponding author: jonas.wolff@mq.edu.au

** corresponding author: nicola.pugno@unitn.it

[a] These authors contributed equally to this work.

1. Inference of mechanical properties of silk anchor parts for *in silico* experiments

Methods. To estimate realistic parameters for our numerical model of silk anchor mechanics, we performed exemplary lateral stress tests of anchors that had been carefully delaminated from polypropylene sheets (see ref. (1) and ref. (2) for more details). Each 7-8 anchors of the basal substrate web builder *H. troglodytes*, the hunting spider *I. villosa* and the aerial web builder *T. plumipes* were glued with cyanacrylate adhesive onto a cardboard strip, such that the central dragline was oriented along the apical edge of the strip. Thereby the glue was spread across one lateral wing of the membrane up to the dragline such that the dragline was fixed (Fig. S1a). The cardboard strip was mounted into the Instron 5542 tensile tester (Instron, Norwood, USA) with a clamp and the stage with an attached ULC-0.5N load cell (Interface, Inc., Scottsdale, AZ, USA) was slowly driven towards the free side of the silk membrane. The lateral edge of the membrane was then glued onto another piece of cardboard that was attached to the load cell, leaving a free membrane sample of 0.11-1.00 mm gauge length (Fig. S1b). The stage was moved slightly downwards to prevent a pre-stress of the silk membrane during adhesive curing. The sample was stretched at a rate of 0.01 mm/s until rupture (Fig. S1c). The process was monitored with a Basler Ace 640×480pix camera (Basler AG, Ahrensburg, Germany) equipped with an extension tube, 1.33× and 0.25× lenses (Navitar, Inc., Rochester, NY, USA) at 15 frames per second to record membrane strain and crack propagation. For each species four tests showed an even fraction of the membrane and were further analysed. To calculate stress, we estimated a cross-sectional area of the membrane $A = w \times t$, where w is the width of the sample and t its thickness. Here, t is given by the observed density of the spinning trajectory (as found in the kinematic analysis), which determines how many layers of piriform silk are applied, with each layer corresponding to the mean diameter of piriform fibres (0.5 µm (2)).

The Young's modulus of the membrane was derived from the initial slope of the stress strain curve (Fig. S1e).

Additional parameters were taken from the literature (3-5).

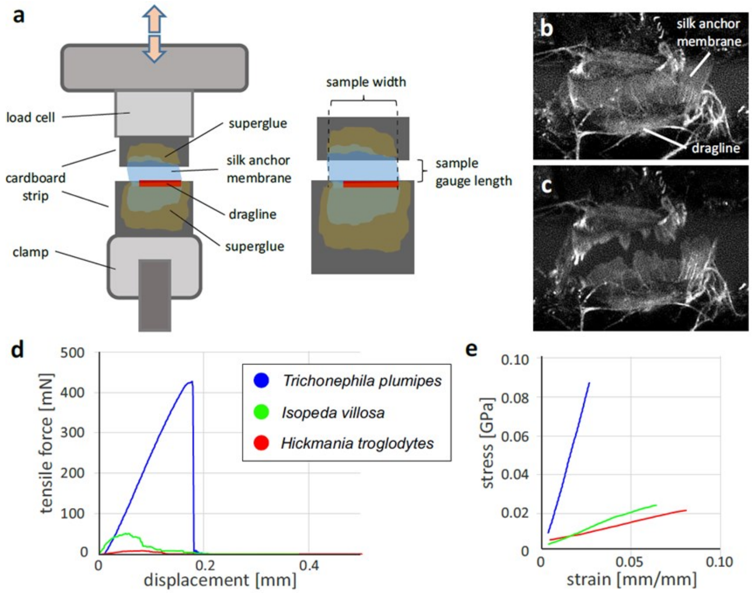

Fig. S1.1. Lateral stress tests of silk anchor membranes. (a) Schematic illustration of membrane stress tests to estimate membrane stiffness and strength. (b) Image of a stretched membrane of a silk anchor of *T. plumipes*. (c) Similar silk membrane after rupture. (d) Exemplary force-displacement plots from membrane tests. (e) Isolated initial slopes of calculated stress-strain curves for used for the estimation of the membrane's Young's modulus.

Results. Parameters estimated from tensile tests are summarized in Tab. S1. Piriform silk membranes generally had a 10-40 times smaller stiffness than dragline silk of these or related species (3-5) (Tabs. 1, S1). Silk membranes of *T. plumipes* were six times stiffer and stronger than the membranes of *I. villosa* and *H. troglodytes*, on average. This may be due to the grid-like overlay of fibres within the membrane (6) caused by the specific back-and-forth spinning pattern in this spider (7).

Tab. S1.1. Estimates of mechanical properties of silk anchor elements from tensile tests.

species	Anchor part	Extensibility [mm/mm]	Strength [GPa]	Young's Modulus [GPa]	Reference
H. troglodytes	membrane [n=4]	0.25 ± 0.09 (mean ± s.d.)	0.035 ± 0.027 (mean ± s.d.)	0.25 ± 0.11 (mean ± s.d.)	this study
	dragline [n=37]	0.1-0.5 (mean ~0.25)	0.5-2.5 (mean ~1.5)	5-20 (mean ~10)	(3)
I. villosa	membrane [n=4]	0.29 ± 0.18 (mean ± s.d.)	0.050 ± 0.018 (mean ± s.d.)	0.22 ± 0.06 (mean ± s.d.)	this study
	dragline	-	-	10	estimated from related taxa (4)
T. plumipes	membrane [n=4]	0.26 ± 0.22 (mean ± s.d.)	0.212 ± 0.076 (mean ± s.d.)	1.68 ± 1.22 (mean ± s.d.)	this study
	dragline [n=66]	0.20 ±0.01	1.000 ±0.004	13.80 ± 3.64	(5) for *T. edulis*

2. *In silico* experiments: parametric study

We consider a 1.4 mm x 1.6 mm rectangular area of thickness $t = 1$ µm and Young's modulus $E_p = 1.68\ GPa$, referred to as *plaque*. We introduce a stiffer element, referred to as *dragline*. The dragline has a Young's modulus of $E_d = 15\ GPa$, a length of $l_d = 0.4$ mm and a width of $w_d = 0.04$ mm. The dragline is inserted at half the width of the attachment, and at a distance from the front border of $d = 0.5\ mm$. The plaque-dragline structure is attached to a rigid substrate. The adhesive energy per unit area is $\phi = 20\ J/m^2$ (estimated by optimizing the overlap of simulated and experimental data). A fixed displacement is imposed to one of the extremities of the dragline, called *front of the dragline*, at different angles. Using the numerical model described in the main manuscript, we have studied how the variation of different geometrical and mechanical parameters affect the adhesive behaviour of the structure. Our goal is to identify which parameters influence the relationship between the structural stiffness and the pulling angle.

2.1. Angle dependency

We vary the pulling angle θ between the extreme values 15° and 165° (representative of the 0° and 180° pulling directions). A difference of less than 2% is found between $F_{max}(120°)$ and $F_{max}(165°)$. The minimum structural stiffness, i.e. the lowest slope of the force-displacement curve, is found for $\theta = 105°$, and for $\theta = 90°$ and $\theta = 165°$ similar stiffnesses are observed. While these observations agree with the experimental results concerning the behaviour of the *H. troglodytes* and the *I. villosa,* the expected structural stiffness of the *T. plumipes* for high pulling angles is smaller. We thus proceed to investigate which parameters influence the structural stiffness *vs* angle behaviour, focusing our studies on $\theta = 90°$ and $\theta = 165°$.

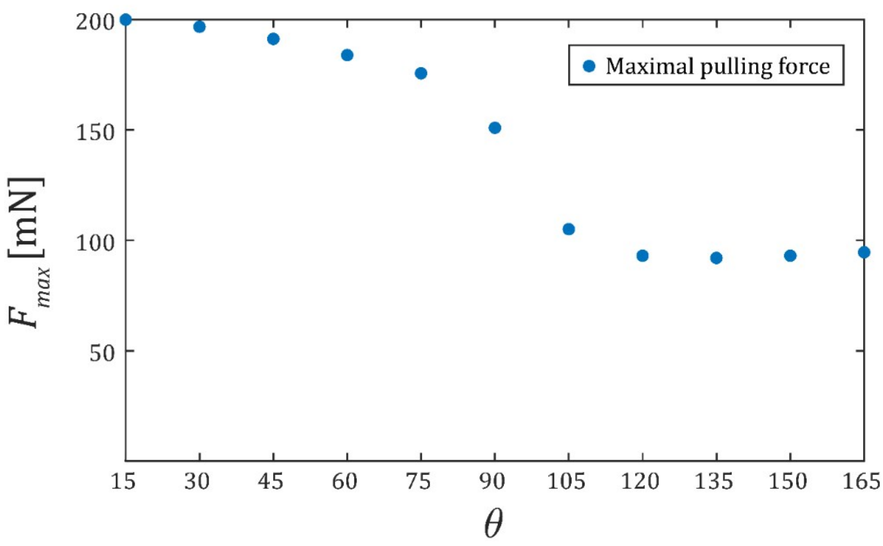

Fig. S1.2. Maximal pulling force F_{max} vs pulling angle θ.

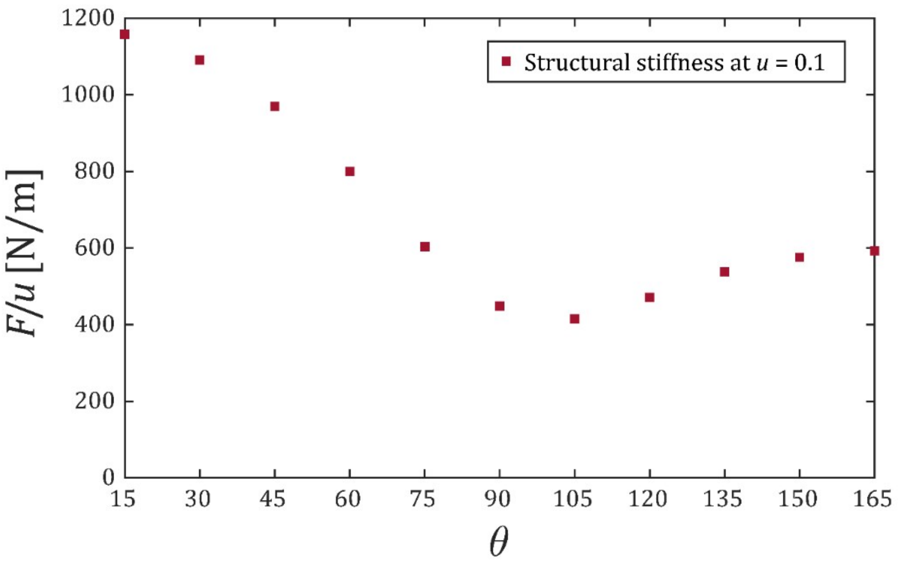

Fig. S1.3. Slope of the force-displacement curve F/u at $u = 0.1\ mm$ vs pulling angle θ.

2.2. Dragline width

We vary the dragline width w_d between the extreme values 0.04 mm and 0.20 mm. For both pulling angles, higher pull-off forces are observed for wider draglines. No changes are observed in the relationship between the force-displacement curve slopes for $\theta = 90°$ and $\theta = 165°$, with $\theta = 165°$ having a higher slope.

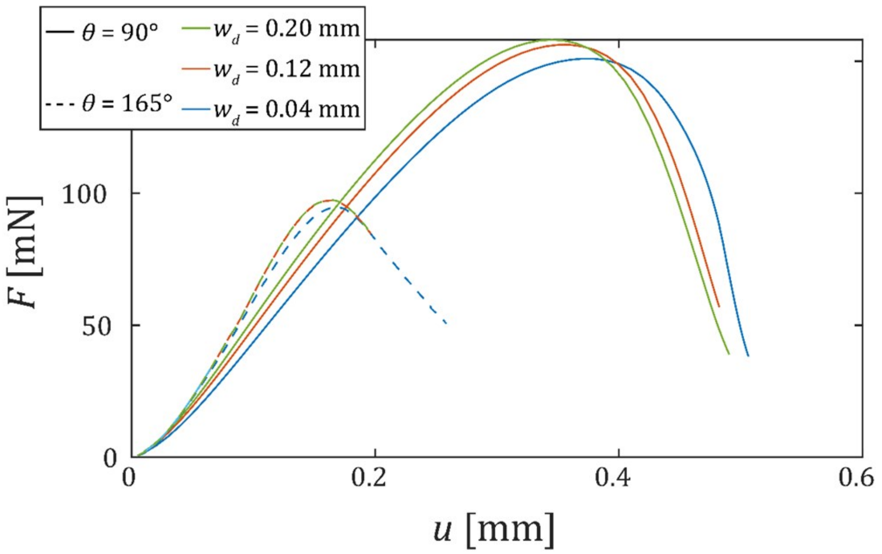

Fig. S1.4. Force vs displacement for different values of the dragline width.

2.3. Dragline length

We vary the dragline length l_d between the extreme values 0.3 mm and 0.6 mm. At a pull-off angle of 90°, higher maximal pull-off forces are observed for shorter draglines. At a pull-off angle of 165° a variation of less than 0.01 mN is observed between the different maximal pull-off forces. No changes are observed in the relationship between the force-displacement curve slopes for $\theta = 90°$ and $\theta = 165°$, with $\theta = 165°$ having a constantly higher slope.Only the two extreme values are shown here for clarity.

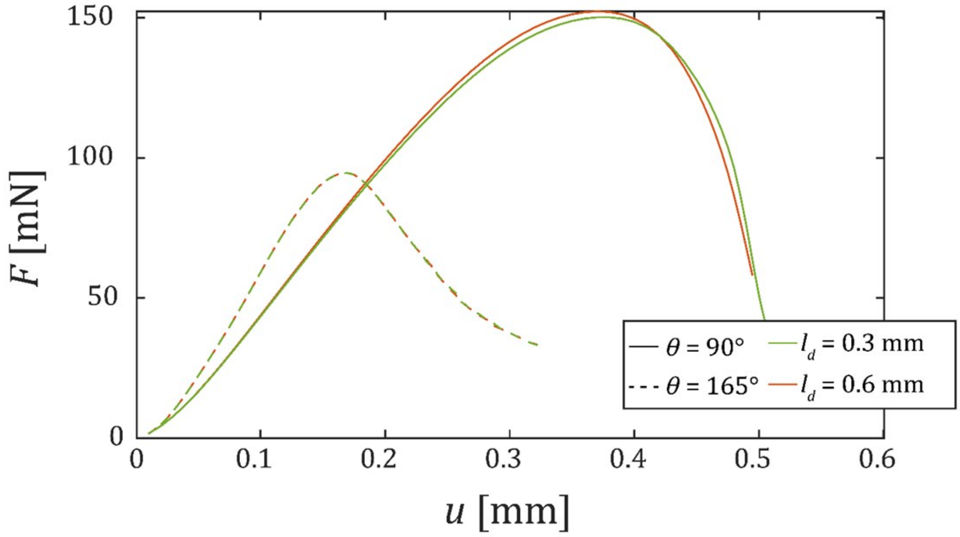

Fig. S1.5. Force vs displacement for different values of the dragline length.

2.4. Adhesive energy per unit area

We vary the adhesive energy per area E_{adh} between the extreme values 40 MPa · mm and 5 MPa · mm. At both pull-off angles, larger maximal pull-off forces at larger displacements are observed for larger adhesive energies per area. No changes are observed in the force-displacement curve slope.

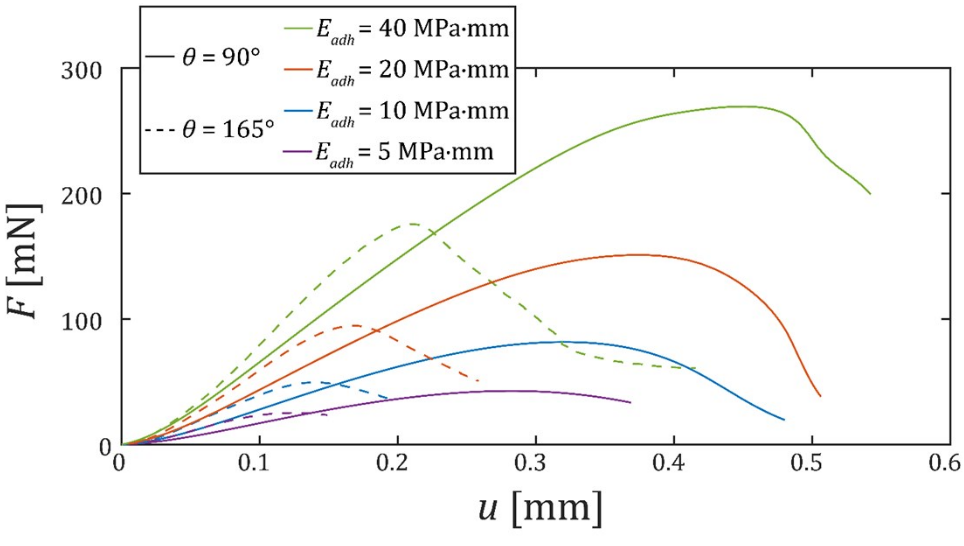

Fig. S1.6. Force vs displacement for different values of the adhesive energy per unit area.

2.5. Thickness

We vary the plaque and dragline thickness t between the extreme values 1.5 µm and 0.1 µm. At both pull-off angles, larger and anticipated maximal pull-off forces are observed for larger thicknesses. No changes are observed in the relationship between the force-displacement curve slope for $\theta = 90°$ and $\theta = 165°$ for $t > 0.5\ \mu m$. A difference between the slopes of less than the 2% is observed for a thickness of $t = 0.1\ \mu m$

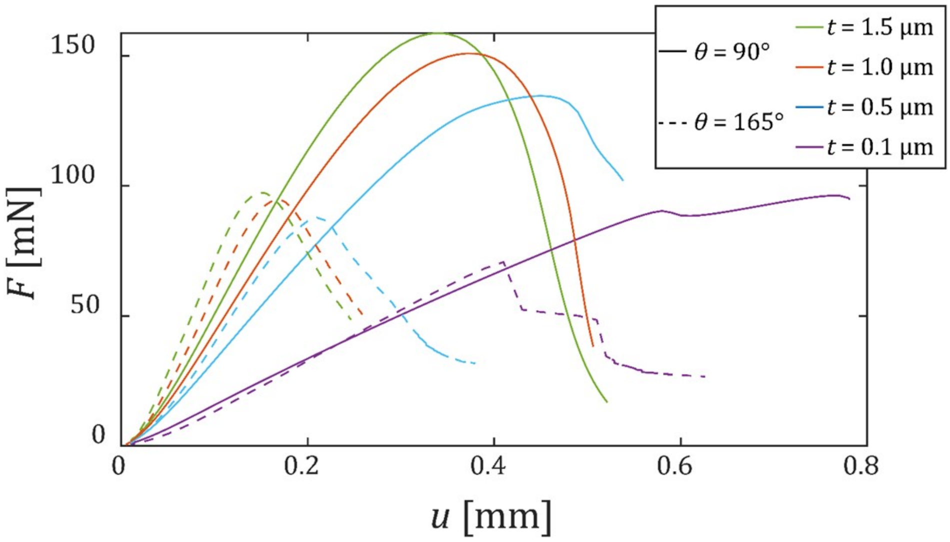

Fig. S1.7. Force vs displacement for different values of the membrane thickness t.

2.6. Silk nonlinear elastic constitutive behaviour

We study the dependence of results on the stress-strain constitutive relation of the material, to mimic the realistic material behaviour of spider silk. The three laws used in this study are a parabolic hardening function, a linear function, and a cubic yielding-hardening function. The thickness is $t = 0.2\ \mu m$. At a pull-off angle of 90°, a nonlinear hardening constitutive law leads to high and anticipated maximal pull-off forces. At a pull-off angle of 165°, a nonlinear hardening constitutive law leads to smaller and anticipated maximal pull-off forces. These behaviours lead to a higher difference between the maximal pull-off forces at $\theta = 90°$ and at $\theta = 165°$ for a nonlinear hardening stress-strain law. No changes are observed in the relationship between the force-displacement curve slopes for $\theta = 90°$ and $\theta = 165°$ for both the hardening and linear stress-strain laws, with $\theta = 165°$ having a constantly higher slope. For a yielding-hardening law, similar slopes are found, with a difference inferior to 4%. . Notice that this is true even if large strains are occurring, as can be seen by the strain map shown in correspondence of the peak force obtained for $\sigma = E\varepsilon - 1.4E\varepsilon^2 + 0.7E\varepsilon^3$.

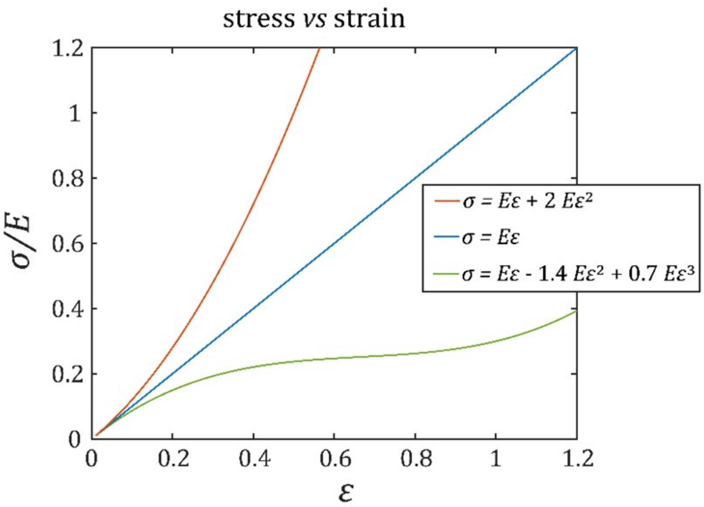

Fig. S1. 8. Stress-strain relationship used in non-linear elastic simulation. A pure hardening law ($\sigma = E\varepsilon + 2E\varepsilon^2$), a linear law ($\sigma = E\varepsilon$) and a yielding-hardening law are considered ($\sigma = E\varepsilon - 1.4E\varepsilon^2 + 0.7E\varepsilon^3$).

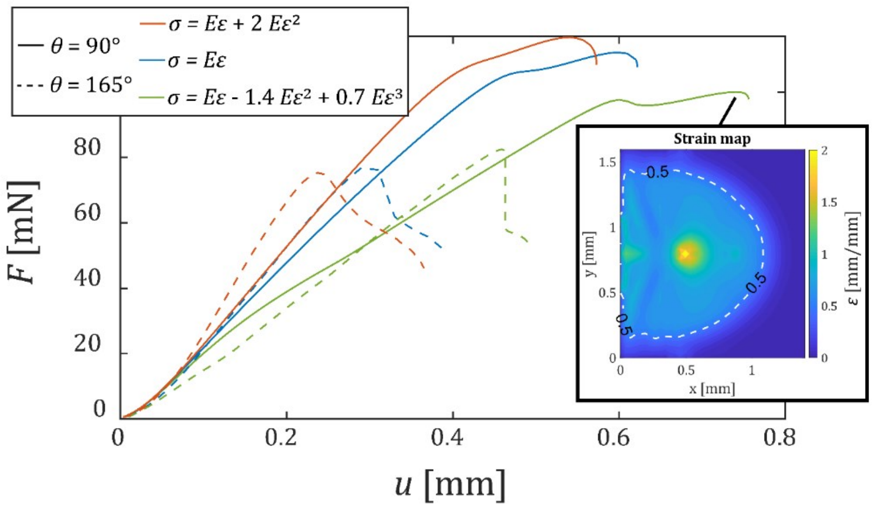

Fig. S1.9. Force vs displacement for different stress-strain relationships. A strain map is shown for the point of maximal pulling force for a yielding-hardening law. Most of the delaminated area is affected by a strain ε>0.5.

2.7. Radius of an initially detached area

We define an initially detached area. The detached area has a Young's modulus $E_b = E_p$ and its centred at the front of the dragline. We vary the radius of the initially detached area r_{det} between the extreme values 0 mm and 4 mm. At a pull-off angle of 90°, slightly smaller maximal pull-off force are observed for larger initially detached areas. The forces converge to the same value for small values of r_{det}, as expected. From fracture mechanics, it is known that the maximal pull-off forces do not depend on the total adhering area, but only from the stressed area. Thus, for an infinite membrane, no difference is observed in the maximal pull-off forces for different values of r_d. The lower maximal pull-off force found for $r_{det} > 4$ mm is caused by border effects, which are involved if the initially detached area is large enough. A cubic force-displacement relationship is observed for larger values of r_{det}. This agrees with the elastic theory of circular elastic membranes. At a pull-off angle of 165° smaller pull-off forces are observed for larger values of r_{det}, and no changes are observed in the relationship between the force-displacement curve slopes, with $\theta = 165°$ having a constantly higher slope than $\theta = 90°$.

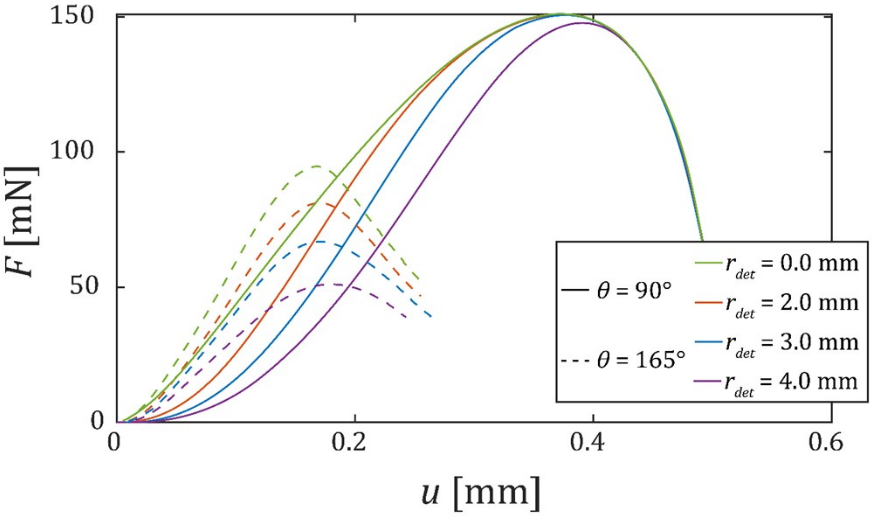

Fig. S1.10. Force vs displacement for different values of the radius of the initially detached area.

2.8. Young's modulus of the initially detached area

We vary the Young's modulus of the initially detached area E_b between the extreme values 0.5 E_p and 0.02 E_p. The detached area has a circular shape, with radius $r_d = 0.4\ mm$ and centred on the front of the dragline. At a pull-off angle of 90°, smaller and delayed maximal pull-off force are observed for lower values of E_b. At a pull-off angle of 165°, delayed maximal pull-off force are observed for lower values of E_b, but no noticeable variation is observed in the maximal pull-off forces. We observe a variation of the slopes of the force-displacement curves: for low values of E_b a lower structural stiffness is observed for high pulling angles, compared to $\theta = 90°$. This is particularly noticeable for values of $E_b < 0.1\ E_p$. This is the only parametric test where this behaviour is observed. We thus assume that in the *T. plumipes* a soft initially detached area is present around the dragline.

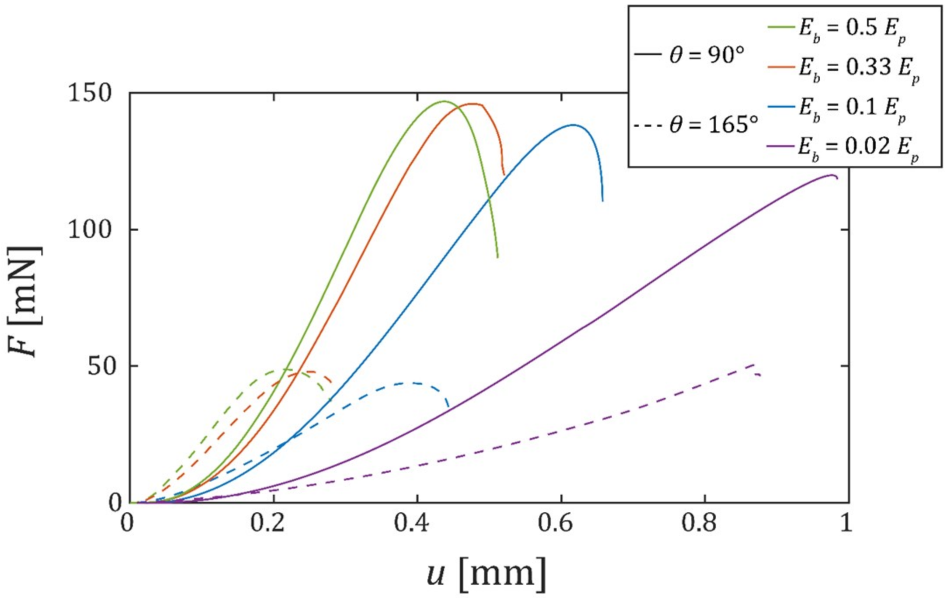

Fig. S1.11. Force vs displacement for different values of the stiffness of the initially detached area.

1.1. Effect of insertion point d

As discussed in *Wolff et al.* (1), a larger d corresponds to larger values of the pulling force for high pulling angles. In this paper, it is also shown that the distance of the insertion point from the edges of the membrane is the main factor determining the maximal adhesive force, since once a border of the attachment peels off there is a drastic decrease in both the pull-off force and the structural stiffness of the adhesive.

Here, for each species, three positions of the dragline are considered. The dragline length l_{dl}, as observed in Figure 2 of the main manuscript, increases for smaller values of d. The set of adopted parameters can be found in **Error! Reference source not found.**.

Tab. S1.2. Geometrical parameters used in the insertion point parametric test.

	l_p (mm)	w_p (mm)	l_{dl} (mm)	d (mm)	b (mm)	r_b (mm)
H. troglodytes	2.4	2.6	1.6 1.2 0.8	0.3 0.5 0.7	-	-
I. villosa	2.1	1.6	1.7 1.3 0.9	0.2 0.4 0.6	(1.0, 0.8)	0.3 0.7 1.1
T. plumipes	1.4	1.5	0.8 0.6 0.4	0.3 0.4 0.5	(0.62, 0.75)	0.45 0.35 0.25

As shown in the main text the effect of d on F_{max} is amplified by the bridge, a structure that was not considered in in *Wolff et al.* (1). In the models of the attachments of the *I. villosa* and *T. plumipes,* there are larger forces for larger values of d at all pulling angles: the presence of an initially detached area surrounding the dragline

allows a redistribution of the stresses. A more centred insertion point and a shorter dragline thus allow for a longer delamination until the first edge is reached, improving the adhesive performance of the attachment.
In the *T. plumipes*, the behaviour at high pulling angles $(\theta = 165°)$ is heavily affected by the dragline insertion point. For $d = 0.3\ mm$ the early detachment of the front border inhibits the effect of the soft bridge, which allows the dragline to align itself to the pulling force, and we thus find the same angle-dependency observed in the *H. troglodytes.*
Finally, larger values correspond to smaller bridges and thus a decrease in the total attached area. However, after Kendall's peeling theory, if we ignore frictional effects, only the adhesive energy per unit area at the delamination front is involved in the detachment (8, 9). There is a proportionality between the pull-off force and work of separation per unit area Φ, which is constant for every set of simulations as explained in the numerical model section of the main manuscript.

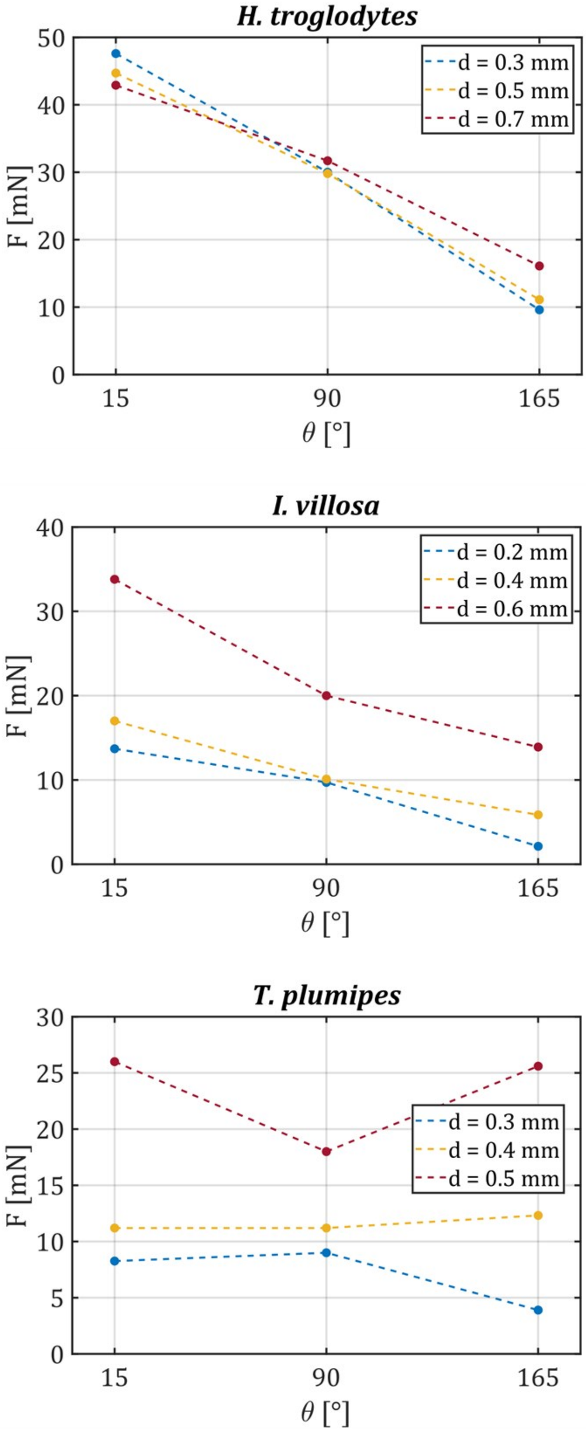

Fig. S1.12. Force vs pulling angle for different values of the insertion point d.

References

1. Wolff JO*, et al.* (2019) Evolution of aerial spider webs coincided with repeated structural optimization of silk anchorages. *Evolution* 73(10):2122-2134.
2. Greco G, Wolff JO, & Pugno NM (2020) Strong and tough silk for resilient attachment discs: the mechanical properties of piriform silk in the spider Cupiennius salei (Keyserling, 1877). *Frontiers in Materials* 7:138.
3. Piorkowski D*, et al.* (2018) Ontogenetic shift toward stronger, tougher silk of a web-building, cave-dwelling spider. *J Zool* 304(2):81-89.
4. Craig HC, Piorkowski D, Nakagawa S, Kasumovic MM, & Blamires SJ (2020) Meta-analysis reveals materiomic relationships in major ampullate silk across the spider phylogeny. *J R Soc Interface* 17(170):20200471.
5. Swanson B, Blackledge T, Beltrán J, & Hayashi C (2006) Variation in the material properties of spider dragline silk across species. *Applied Physics A* 82(2):213-218.
6. Wolff JO, Grawe I, Wirth M, Karstedt A, & Gorb SN (2015) Spider's super-glue: thread anchors are composite adhesives with synergistic hierarchical organization. *Soft Matter* 11(12):2394-2403.
7. Wolff JO & Herberstein ME (2017) 3D-printing spiders: back-and-forth glue application yields silk anchorages with high pull-off resistance under varying loading situations. *J R Soc Interface* 14:20160783.
8. Kendall K (1975) Thin-film peeling - The elastic term. *Journal of Physics D: Applied Physics* 8(13):1449-1452.
9. Chen B, Wu P, & Gao H (2008) Hierarchical modelling of attachment and detachment mechanisms of gecko toe adhesion. *Proceedings of the Royal Society A: Mathematical, Physical Engineering Sciences* 464(2094):1639-1652.